Nuclear Inst. and Methods in Physics Research, A 909 (2018) 456–459

Contents lists available at ScienceDirect

Nuclear Inst. and Methods in Physics Research, A

journal homepage: www.elsevier.com/locate/nima

Initial beam dynamics simulations of a high-average-current field-emission electron source in a superconducting radiofrequency gun

O. Mohsen [a,*], I. Gonin [b], R. Kephart [b], T. Khabiboulline [b], P. Piot [a,b], N. Solyak [b], J.C. Thangaraj [b], V. Yakovlev [b]

[a] Department of Physics and Northern Illinois Center for Accelerator & Detector Development, Northern Illinois University, DeKalb, IL 60115, USA
[b] Fermi National Accelerator Laboratory, Batavia, IL 60510, USA

ARTICLE INFO

Keywords:
Superconducting radiofrequency cavity
High-current electron source
Field emission

ABSTRACT

High-power electron beams are sought-after tools in support to a wide array of societal applications. This paper explores the production of high-power electron beams by combining a high-current field-emission electron source to a superconducting radio-frequency (SRF) cavity. We especially carry out beam-dynamics simulations that demonstrate the viability of the scheme to form ~300 kW average-power electron beam using a 1+1/2-cell SRF gun.

© 2018 The Authors. Published by Elsevier B.V. This is an open access article under the CC BY-NC-ND license (http://creativecommons.org/licenses/by-nc-nd/4.0/).

1. Introduction

Electron accelerators are finding an increasing number of applications in our society. Many of these applications require high-average-power beams produced at low cost and within compact footprints. A superconducting radiofrequency (SRF) cavity combined with a high-current electron source offers a promising path toward the generation of multi MeV Ampère-class electron beams within meter-scale footprints [1].

Thermionic cathode are well established as a robust technology but their operation in RF guns is hindered by back bombardments and beam losses [2]. The mitigation of back bombardment is challenging and its total suppression has been elusive so far. Another complication associated to thermionic cathode regards their high-operating temperatures which pose engineering challenges when combined with the cryogenic temperatures necessary to SRF cavities operation [3]. Likewise, photoemission sources are capable of producing bright electron beams but require a laser system to trigger the emission which increases the overall complexity of the source.

Field-emission (FE) sources are appealing due to the simplified setup (no auxiliary system, no heat load). The field-emission process – a macroscopic manifestation of quantum tunneling – occurs when the emitting surface is subjected to a strong electric field. The theory behind FE is well established and the current density is related to the applied electric field $E_z(t)$ via the Fowler–Nordheim's law [4,5]

$$j(t) = A(\Phi)[\beta_e E_z(t)]^2 e^{\frac{-B(\Phi)}{\beta_e E_z(t)}}, \quad (1)$$

where the parameters $A(\Phi)$ and $B(\Phi)$ depend on the work function Φ of the material and β_e is the field enhancement factor. The time-dependent field results in a modulated current density so that bunched electron beams are generated; see Fig. 1(a). For a field with the harmonic time dependence $E_z(t) = E_0 \sin(\omega t)$, the root-mean square (RMS) duration of the emitted bunches (close to the cathode surface) is $\sigma_t \simeq \omega^{-1}\sqrt{\beta_e E_0/B(\Phi)}$ so that, for a given surface material and applied field, higher frequencies yield shorter bunches. Fig. 1(b) displays the bunch duration and current density evolution as a function of the applied peak electric field for parameters comparable to the one considered below. In the recent years, FE has been extensively investigated as electron sources for bright [6] or high-current [7] electron beams.

2. Concept

Fermilab is developing technologies to support of compact SRF MW-class electron accelerators. A critical component toward the realization of small footprint is the use of conduction cooling based on cryocooler [1] which circumvents the use of large cryogenic infrastructures. A possible approach combines a high-current electron source to a 650 MHz SRF cavity. In order to reach the needed energy of ~ 10 MeV, a 4 + 1/2-cell SRF cavity is envisioned. In a first phase a 1 + 1/2-cell prototype implementing conduction cooling will be tested and the produced electron beam characterized. In its nominal configuration the SRF cavity if foreseen to incorporate a thermionic electron source.

* Corresponding author.
E-mail address: omohsen@niu.edu (O. Mohsen).

https://doi.org/10.1016/j.nima.2018.01.018
Received 20 November 2017; Received in revised form 14 December 2017; Accepted 8 January 2018
Available online 11 January 2018
0168-9002/© 2018 The Authors. Published by Elsevier B.V. This is an open access article under the CC BY-NC-ND license (http://creativecommons.org/licenses/by-nc-nd/4.0/).

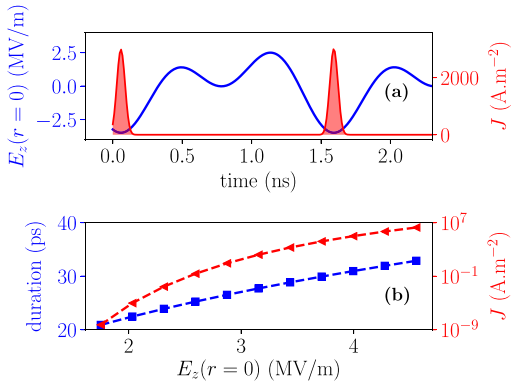

Fig. 1. Axial electric field applied on the cathode (blue trace) and the emitted current density (red shaded curve) (a). Evolution of the current density peak value (squares) and RMS electron pulse duration (triangles) as function of the applied peak field (b). The peak-field configuration and associated parameters are detailed in Section 2. Note that these are ideal numbers calculated at the cathode surface without accounting for possible saturation effects of the emission process.

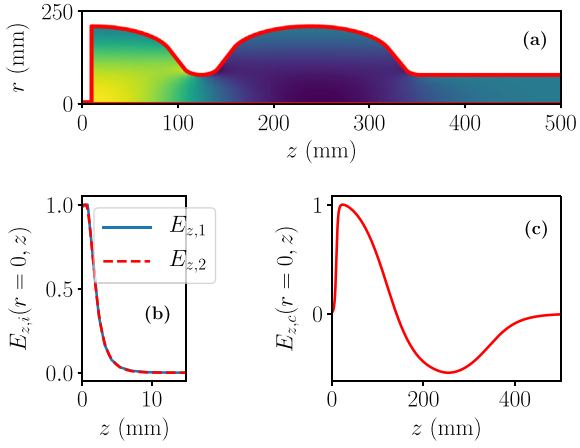

Fig. 2. Geometry of the SRF cavity (red trace) with field distribution $E_z(r,z)$ (a), axial fundamental $E_{z,1}(r=0,z)$ and harmonic $E_{z,2}(r=0,z)$ electric fields in the vicinity of the cathode surface and axial field $E_{z,c}(r=0,z)$ along the $1+1/2$-cell cavity (c). All the field are normalized to their peak amplitudes.

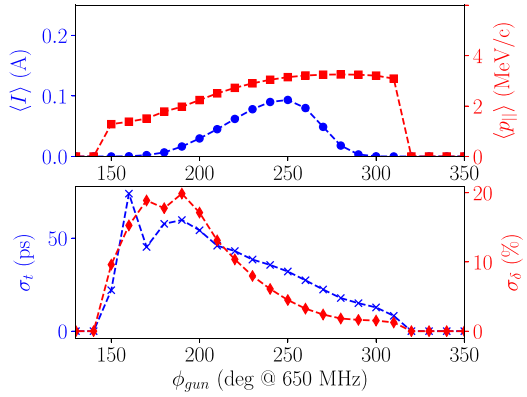

Fig. 3. Evolution of the average beam current (blue) and average longitudinal momentum (red) (top) and RMS bunch duration (blue) and fractional momentum spread (red) (bottom) versus ϕ_{gun}. (For interpretation of the references to color in this figure legend, the reader is referred to the web version of this article.)

However a FE-source option is also under consideration pending the associated technological risks can be mitigated. In this paper, we use a simple cavity model for a 1+1/2-cell SRF gun with its geometry obtained

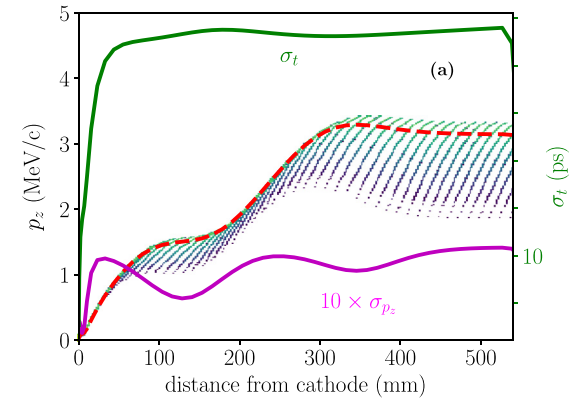

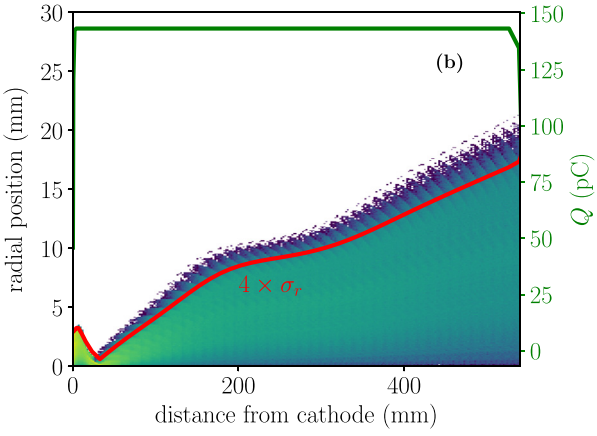

Fig. 4. Longitudinal momentum (top) and radial (lower) distribution along the SRF cavity (color density histograms). The traces on the top plot represent the RMS bunch duration (green), the mean longitudinal momentum (dash red) and the 10-times RMS momentum (magenta). The traces on the lower plot respectively show the 4-times RMS radius (red) and the bunch charge (green). (For interpretation of the references to color in this figure legend, the reader is referred to the web version of this article.)

from a frequency scaling the 1.3 GHz TESLA-cavity geometry [8] such to resonate at 650 MHz; see Fig. 2(a). The model was simulated with the SUPERFISH software [9]. One peculiarity of the SRF-gun design regards the addition of an aperture on its backplate to allow for the high-current electron source to be recessed; see [10]. This setup enables the cathode to be located a few mm behind the SRF-cavity backplate and subjected to a tailored electromagnetic field as discussed in Refs. [3,11]. Such a configuration has several advantages: (*i*) it allows for the independent control of the emission and acceleration processes (as the fields applied to the cathode surface can have their amplitudes and phases tuned independently from the field in the SRF cavity), and (*ii*) it also avoids direct exposure of the cathode to the SRF-cavity field thereby lowering risks associated to vacuum contamination. In our investigation, we consider a setup similar to the one described in [10] where the cathode is located at the extremity of a small RF gap with net on-axis axial electromagnetic field given by the superimposition of the SRF cavity field with a local fundamental and a second-harmonic fields

$$E_z(z,t) = E_{z,c}(z)\sin(2\pi f t) + E_{z,1}(z)\sin(2\pi f t + \varphi_1) + \\ + E_{z,2}(z)\sin(4\pi f t + \varphi_2), \quad (2)$$

where $f = 650$ MHz is the fundamental frequency, $E_{z,c}$ is the penetrating field from the SRF cavity while $E_{z,i}$ and φ_i are respectively the field amplitudes and phases of the fundamental ($i = 1$) and harmonic ($i = 2$) fields produced by a bimodal cavity [11]. The axial coordinate z is referenced w.r.t. the cathode surface. As a first iteration the bimodal cavity designed in support of the thermionic-source option was used

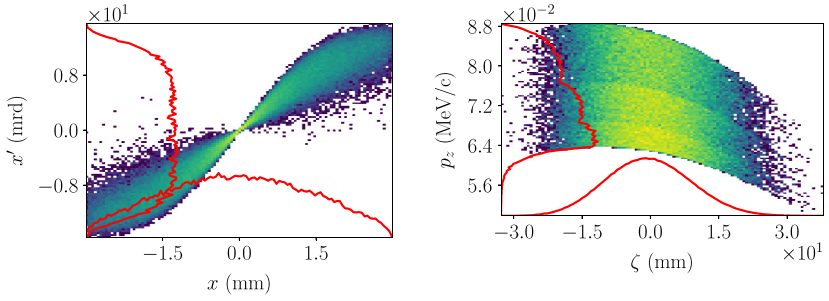

(a) $z = 1$ mm.

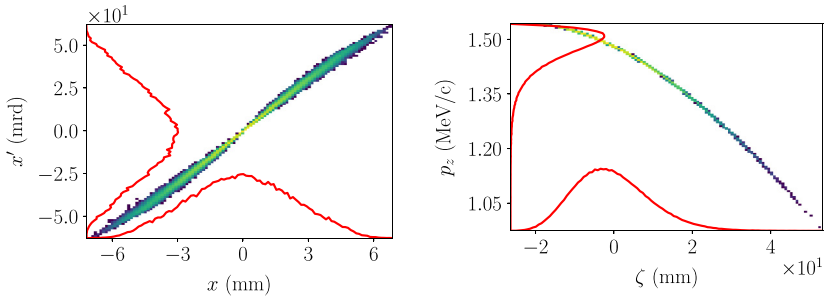

(b) $z = 124$ mm.

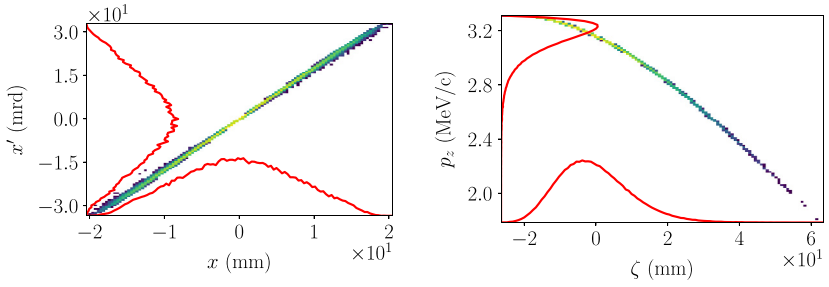

(c) $z = 543$ mm.

Fig. 5. Simulated transverse trace-space (left) and longitudinal phase-space (right) distributions at three axial locations z along the accelerator beamline (z is referenced w.r.t. the cathode surface). The false color density represents the number of macroparticles (i.e. the charge) while the traces are the corresponding projections along each axis.

and its field accordingly scaled. Fig. 2(b) displays the normalized axial fundamental and second-harmonic fields supported by the bi-modal cavity as modeled with SMASON [12]. In order to mimic the boundary conditions imposed by the RF gap on SRF-cavity field, a cylindrical pipe was added at the extremity of the cavity $z \in [0, 10]$ mm. The field in the 1.3 GHz cavity was also simulated with the finite-difference time-domain (FDTD) axi-symmetric program SPIFFE [13] to provide two-dimensional (r, z) field maps for the beam-dynamics simulations.

3. Beam-dynamics simulations

3.1. Methods

The beam-dynamics performances of the FE source were explored via numerical simulations carried out with SPIFFE which incorporates a particle-in-cell (PIC) algorithm. The field supported by the bimodal cavity were modeled from their axial spatial profile $E_i(z)$ and the associated transverse electromagnetic fields are obtained within SPIFFE using the paraxial approximation. However, given the possible large transverse orbit excursion in the SRF cavity, the SRF-cavity field is modeled by the time-dependent 2-D field map obtained using SPIFFE ran in the electromagnetic mode.

The FE process based on Eq. (1) is implemented in SPIFFE. The cathode is located at $z = 0$ and its outer radius was taken to be 3 mm. The work function was taken to be $\Phi = 4.5$ eV (carbon-based field emitter) and a field enhancement factor $\beta_e = 700$ was selected which represent an upper value for, e.g., in carbon-nanotube field emitters [7]. We note that lower field-enhancement factors could be employed at the expense of increasing the peak field on the cathode such an optimization will be performed together with optimizing possible solutions for the bimodal-cavity design [14]. In order to reduce the simulation time, the macro-particles describing the electron-bunch distribution represent 10 000 electrons. Owing to the self-phasing of the field-emission process, our simulation use the phase of the SRF cavity as a reference and the phases of the fields supported by the bimodal cavity are referenced w.r.t. the SRF-cavity phase; see Eq. (2). The phases and amplitude of the fundamental and harmonic fields in the RF gap were all set to be equal; specifically $\varphi_1 = \varphi_2 \equiv \phi_{gun}$ and $E_{z,1}(0) = E_{z,2}(0) = 2$ MV/m.

3.2. Results

A critical parameters to the beam dynamics is the selected emission "launch" phase ϕ_{gun} w.r.t. the SRF cavity field. Fig. 3 displays the evolution of the final beam energy, and other longitudinal-phase-space parameters as a function of ϕ_{gun}. The results indicate that a maximal average current of $\langle I \rangle \simeq 93$ mA can be attained with a mean momentum of $\langle p_z \rangle \simeq 3.15$ MeV/c for a launch phase of $\phi_{gun} = 250°$. Fig. 1(a) gives the corresponding axial field on the cathode as a function of time with the emitted current density. The corresponding bunch duration and fractional momentum spread are respectively $\sigma_t \simeq 35$ ps and $\sigma_\delta \simeq$

5%. Our simulation indicate that space-charge effects are insignificant [consistent with the peak current of $\hat{I} \sim Q/\sigma_t \sim \mathcal{O}(10\ \mathrm{A})$]. Likewise, the emission is not space-charge-limited. The attained set of beam parameters correspond to an average-power of $\langle P \rangle \simeq 292$ kW. For this maximum-current launch phase our simulation did not result in any back bombardment nor particle losses which, given the number of macroparticle used in our simulation $N_m \simeq 90\,000$, sets an upper limit for the relative charge loss of $Q_{loss}/Q < 1/N_m \simeq 1.11 \times 10^{-5}$. The latter value represents an upper limit for the average power loss of $\langle P_{loss} \rangle \simeq Q_{loss}/Q\langle P \rangle < 3.2$ W within the cryogenic budget. It should be stressed that the latter value is limited by the reduced number of macroparticle used in our simulation. Carrying out large-scale simulations, once the design is refined, will provide a better resolution on the power loss.

The corresponding evolutions of the longitudinal momentum and radial distributions during acceleration in the SRF cavity appear in Fig. 4 along with associated RMS quantities. The bunch duration reaches its final value within the first half cell of the SRF cavity while the fractional energy spread continuously increases as the longitudinal-phase-space nonlinearity impressed by the RF waveform accumulates during the acceleration process. Given the absence of focusing the 4-σ_r beam radius continuously increases to its final value of $4\sigma_r \simeq 17$ mm at the exit of the SRF-cavity. While such a value is well within the aperture sets by the beamline vacuum-pipe radius, schemes to mitigate the beam size growth will be explored (these include modifying the 1/2-cell of the SRF cavity to introduce some RF focusing).

A sequence of snapshots of the longitudinal phase spaces (ζ, δ) and transverse trace spaces (x, x') simulated at three different axial locations are displayed in Fig. 5. The longitudinal phase space presents a significant quadratic correlation from the early stage (starting from the exit of the bimodal cavity) while the transverse trace space displays large correlated divergences which decrease as the beam is accelerated in the SRF gun.

4. Summary

In summary the exploratory simulations presented in this paper suggests that the use of a field-emission source in the proposed SRF-gun prototype could be a viable option as far as the beam dynamics is concerned. Additionally, our investigations shows that some of the crucial parameter, e.g., the electron-bunch duration, have converged to their final values downstream of the 1/2-cell thereby suggesting that the $1 + 1/2$ demo source will provide valuable information that could guide the design of the foreseen MW-class SRF gun based on a $4 + 1/2$-cell SRF cavity. Further improvements of the modeling should include the precise optimization of the bimodal cavity to produce the required field on the cathode (e.g. to possibly accommodate cathode materials with lower enhancement factors), along with the optimization of the field profile in the SRF cavity. Nevertheless, our study provides some impetus to further investigate the technological aspects associated to the inclusion of a field-emission source and especially identify cathode materials compatible with operation in the SRF cavity. Possible contenders, beside the CNT cathodes discussed earlier, include niobium nano-ribbons [15] and nanocrystalline planar cathodes [16].

Acknowledgments

This work was supported by the US Department of Energy (DOE) under contract DE-SC0018367 with Northern Illinois University. Fermilab is managed by the Fermi Research Alliance, LLC for the U.S. Department of Energy Office of Science Contract number DE-AC02-07CH11359.

References

[1] R. Kephart, et al., Srf compact accelerator for industry and society, in: Proceedings of SRF2015, Whistler, BC, Canada, 2015, pp. 1467–1469.
[2] T. Kii, et al., Experiment and analysis on back-bombardment effect in thermionic rf gun, Nucl. Instrum. Methods A 475 (2001) 588–592.
[3] J. Lewellen, J. Noonan, Field-emission cathode gating for rf electron guns, Phys. Rev. ST Accel. Beams 8 (3) (2005) 033502.
[4] R.H. Fowler, L. Nordheim, Electron emission in intense electric fields, in: Proc. of the Royal Society of London A, vol. 119, The Royal Society, 1928, pp. 173–181.
[5] J.W. Wang, G.A. Loew, Field emission and rf breakdown in high-gradient room-temperature linac structure, in: report SLAC-PUB-7684 (unpublished), 1997.
[6] J. Jarvis, et al., Resonant tunneling and extreme brightness from diamond field emitters and carbon nanotubes, J. Appl. Phys. 108 (2010) 094322.
[7] P. Piot, et al., Operation of an ungated diamond field-emission array cathode in a l-band radiofrequency electron source, Appl. Phys. Lett. 104 (2014) 263504.
[8] B. Aune, et al., Superconducting tesla cavities, Phys. Rev. ST Accel. Beams 3 (2000) 092001.
[9] K. Halbach, R. Holsinger, Superfish: A computer program for evaluation of rf cavities with cylindrical symmetry, Part. Accel. 7 (1976) 213–222.
[10] N. Sipahi, et al., Rf design of a high average beam-power srf electron source, in: 7th International Particle Accelerator Conference (IPAC'16), Busan, Korea, May 8–13, 2016, JACOW, Geneva, Switzerland, 2016, pp. 2289–2291.
[11] J. Edelen, et al., Electron back-bombardment and mitigation in a short gap thermionic cathode rf gun, IEEE Trans. Nucl. Sci. 61 (2014) 830.
[12] D. Myakishev, M. Tiunov, V. Yakovlev, Code supersam for calculation of electron guns with high beam area convergence, in: Proceedings of XV-th International Conference on High Energy Accelerators July 20–24, 1992, Hamburg, Germany. Internat. J. Modern Phys. A 2B (1993) 915–917.
[13] M. Borland, Summary of equations and methods used in SPIFFE, Advanced Photon Source, internal report 92-2.
[14] S.V. Kuzikov, et al., Asymmetric bimodal accelerator cavity for raising rf breakdown thresholds, Phys. Rev. Lett. 104 (2010) 214801.
[15] U. Patel, et al., Synthesis and superconducting properties of niobium nitride nanowires and nanoribbons, Appl. Phys. Lett. 91 (2007) 162508.
[16] S. Baryshev, et al., Planar ultrananocrystalline diamond field emitter in accelerator radio frequency electron injector: Performance metrics, Appl. Phys. Lett. 105 (2014) 203505.